C-terminal domain of eukaryotic initiation factor 5 promotes start codon recognition by its dynamic interplay with eIF1 and eIF2β

Rafael E. Luna[1,11], **Haribabu Arthanari**[1,11], **Hiroyuki Hiraishi**[2], **Jagpreet Nanda**[3], **Pilar Martin-Marcos**[4], **Michelle A. Markus**[1,8], **Barak Akabayov**[1], **Alexander G. Milbradt**[1], **Lunet E. Luna**[1,5,9], **Hee-Chan Seo**[6], **Sven G. Hyberts**[1], **Amr Farmy**[1], **Mikhail Reibarkh**[1,10], **David Miles**[2], **Patrick R. Hagner**[1], **Eilzabeth M. O'Day**[1], **Tingfang Yi**[1], **Assen Marintchev**[7], **Alan Hinnebusch**[4], **Jon Lorsch**[3], **Katsura Asano**[2], and **Gerhard Wagner**[1,*]

[1]Department of Biological Chemistry and Molecular Pharmacology, Harvard Medical School, Boston, MA 02115

[2]Molecular, Cellular and Developmental Biology Program, Division of Biology, Kansas State University, Manhattan, KS 66506

[3]Department of Biophysics and Biophysical Chemistry, Johns Hopkins University School of Medicine, Baltimore, MD 21205

[4]Laboratory of Gene Regulation and Development, Eunice Kennedy Shriver National Institute of Child Health and Human Development, National Institutes of Health, Bethesda, MD 20892

[5]Department of Chemical Engineering, Massachusetts Institute of Technology, Cambridge, MA 02139

[6]Department of Molecular Biology, University of Bergen, Bergen, Norway N-5020

[7]Department of Physiology and Biophysics, Boston University School of Medicine, Boston, MA 02118

SUMMARY

Recognition of the proper start codon on mRNAs is essential for protein synthesis, which requires scanning and involves eukaryotic initiation factors (eIFs) eIF1, eIF1A, eIF2 and eIF5. The carboxyl-terminal domain (CTD) of eIF5 stimulates 43S preinitiation complex (PIC) assembly; however, its precise role in scanning and start codon selection has remained unknown. Using nuclear magnetic resonance (NMR) spectroscopy, we identified the binding sites of eIF1 and eIF2β on eIF5-CTD and find that they are partially overlapped. Mutating select eIF5 residues in the common interface specifically disrupts interaction with both factors. By abrogating eIF5-CTD binding to eIF2β, genetic and biochemical evidence indicate that these eIF5-CTD mutations

[*]Corresponding author: gerhard_wagner@hms.harvard.edu.
[8]Present address: R&D Division, Bruker BioSpin Corporation, Billerica, MA 01821
[9]Present address: Department of Chemical and Biomolecular Engineering, University of California Berkeley, Berkeley, CA 94720
[10]Present address: Merck & Co. Inc, Rahway, NJ 07065
[11]These authors contributed equally to this work.

SUPPLEMENTAL INFORMATION Supplemental Information includes seven figures, five tables, Extended Experimental Procedures Extended Results and Extended Discussion.

impair start codon recognition and impede eIF1 release from the PIC. This study provides mechanistic insight into the novel role of eIF5-CTD's dynamic interplay with eIF1 and eIF2β in switching PICs from an open to closed state at start codons.

Keywords

Translation initiation; eukaryotic translation initiation factors; eIF1; eIF1A; eIF2; eIF2β; eIF5; start codon recognition; scanning; 40S ribosome; PIC; NMR; SAXS; mRNA

INTRODUCTION

To achieve accurate selection of the AUG-start codon, the scanning PIC is thought to exist in equilibrium between two conformations, mediated by initiation factors: open, scanning–competent, and closed, scanning–incompetent (Pestova and Kolupaeva, 2002). Recently a crystal structure of the *Tetrahymena thermophila* 40S subunit along with eIF1 was determined, which is strategically located near the P-site (Rabl et al., 2011) consistent with previous hydroxyl-radical footprinting studies (Lomakin et al., 2003). In this crystal structure, the head of the 40S in different space groups has been found in different conformations relative to the body. This may indeed be related to the two inferred states; however, the detailed mechanism of start codon recognition caused by the dynamic interplay of initiation factors with the mRNA and the ribosome will require additional investigations with a wide range of biophysical/biochemical methods along with validation in both *in vitro* and *in vivo* assays. Here, we seek to elucidate the mechanisms of start codon recognition.

Studies on yeast factors have suggested a model for initiation factor-mediated conformational changes of the ribosome during the process of scanning and start codon recognition (Asano and Sachs, 2007; Hinnebusch, 2011): (i) eIF1 and eIF1A stabilize the open complex with Met-tRNA$_i^{Met}$ loaded on the P-site. Here, the globular part of eIF1A occupies the A-site while its C-terminal tail (CTT) extends into the P-site (Yu et al., 2009), and eIF1 binds on the 40S next to the Met-tRNA$_i^{Met}$ (Lomakin et al., 2003). (ii) eIF5 induces the hydrolysis of GTP bound to eIF2 as a GTPase activating protein (GAP) upon or subsequent to mRNA binding to the PIC; however, the resulting GDP and P_i are thought to remain bound to eIF2 in the scanning PIC. P_i release is the rate-limiting step of the PIC in response to AUG selection. (iii) AUG recognition and tighter Met-tRNA$_i^{Met}$ binding triggers the transition to the closed state but requires eIF1 dissociation and ejection of the C-terminal tail of eIF1A from the P-site. (iv) eIF1 dissociation enables gated release of P_i, which effectively ends the scanning mechanism. The dissociation of eIF1 with concomitant P_i release signifies the first irreversible step in translation initiation; hence, we asked whether eIF5-CTD serves a regulatory function in the ejection of eIF1 from PICs at start codons.

Capitalizing on different eIF1A dissociation kinetics between the open and closed states, individual mutations altering eIF1A or eIF5 (within its NTD) were shown to manipulate the closed and open states of the AUG- or UUG-bound PIC (Maag et al., 2006). Any mutation that favors the closed PIC and allows initiation at a faulty UUG codon would promote translation initiation at the expense of lower fidelity, leading to a suppressor of initiation codon mutation (Sui⁻) phenotype, whereas a mutation that favors the open complex and block faulty initiation at a UUG codon would increase the fidelity of translation initiation, a suppressor of Sui⁻ (Ssu⁻) phenotype (Saini et al., 2010). Thus Sui⁻ mutations stabilize the closed state, whereas Ssu⁻ mutations favor the open state of the PIC (summarized in Table S1).

eIF5 is necessary for 60S ribosomal subunit joining, which is ultimately mediated by eIF5B and occurs only after start codon recognition and the cessation of scanning (Pestova et al., 2000). The best characterized function of eIF5 is to serve, through its N-terminal domain (eIF5-NTD; residues 1-170), as the GAP for the eIF2-TC (Conte et al., 2006), which is critical for start codon recognition. The CTD of eIF5 plays a role in assembly of the PIC by stabilizing interactions among eIF1, eIF2 and eIF3 in the multifactor complex (MFC) (Asano et al., 2000; Sokabe et al., 2011). However, the interactions of eIF5-CTD with these other factors have not been fully characterized biophysically, and it was unknown whether the eIF5-CTD functions in scanning or AUG selection.

In order to elucidate critical initiation factor interactions required to promote start codon recognition and grasp a better understanding of the mechanism leading to the cessation of the scanning process, we employ an interdisciplinary approach to examine the dynamic function of the eIF5-CTD in conjunction with release of eIF1 from PICs, which signifies the first committed step in translation initiation. We identify overlapping surfaces on eIF5-CTD that bind to eIF1 and an N-terminal lysine-rich region of eIF2β. Using NMR spectroscopy, small-angle X-ray scattering (SAXS) and isothermal titration calorimetry (ITC), we characterize these interactions and obtain a model for the eIF1:eIF5-CTD complex, which is congruent with the eIF1:40S structure. We unveil a common interface on eIF5-CTD that is important for start codon recognition, and show that mutating these surface residues disrupt its binding to eIF1 and eIF2β. Surprisingly, our biochemical and genetic studies in yeast show that the CTD of eIF5 ends scanning by stabilizing the closed, scanning-arrested state of the PIC at start codons. We suggest that the NTD (GAP) and CTD (HEAT) of eIF5 serve a dual role in promoting the shift to the closed conformation in response to start codon selection. The eIF5-CTD interaction with eIF2β facilitates the subsequent release of eIF1 and ends the scanning process, while priming the PIC for eventual translation initiation.

RESULTS

Unveiling the surface of eIF5-CTD that binds to eIF1 and characterization of this interface

In order to map the surface of human eIF5-CTD that interacts with human eIF1, the chemical shift perturbation (CSP) assay was performed using uniformly ^{15}N-labeled human eIF5-CTD domain and unlabeled eIF1 (Figure S1A-B). We performed backbone resonance assignments of eIF5-CTD at 200 mM NaCl. 95% of the eIF5-CTD backbone resonance signals were assigned using the program IBIS, along with standard triple-resonance experiments (Hyberts and Wagner, 2003; Marintchev et al., 2007). eIF1-induced chemical shift perturbations of eIF5-CTD backbone amide signals were mapped onto the surface of eIF5-CTD (Figure 1A-D). We also used the NMR backbone resonance assignments of human eIF1 and the CSP assay (Fletcher et al., 1999) to map the human eIF5-CTD binding surface on human eIF1 (Figure 1E-F & Figure S1C-D). The binding surface on eIF1's body includes a glycine (G101), along with both charged and hydrophobic residues (D53 and F63) (Figure 1E-F).

We employed paramagnetic relaxation enhancement (PRE) measurements to generate distance restraints between eIF1 and eIF5-CTD. MTSL spin labels were attached to single-cysteine mutations of eIF1 and distance-dependent broadening of eIF5-CTD amide backbone resonances in complex with eIF1 were measured in ^{15}H-^{1}H TROSY HSQC spectra yielding distance restraints within a 20 Å radius (Figure S2A, green spectra). Addition of ascorbic acid reduces the MTSL nitroxide label restoring the intensity of the resonances previously broadened by the MTSL (Figure S2A, purple spectra). In Figure S2C-G, histograms show the intensity ratios of peaks in eIF5-CTD spectra in the presence (Figure S2A; green spectra) and absence of paramagnetic broadening (Figure 2A; purple spectra). This NMR PRE approach accomplishes two goals: 1) It provides distance restraints (< 20 Å)

between five positions on eIF1 and the multiple eIF5-CTD residues. 2) It confirms that the surface on eIF5-CTD affected by eIF1 binding is at/near the binding interface. Distance restraints derived from the PRE experiments (Battiste and Wagner, 2000), along with the chemical shift perturbation data, were used in the HADDOCK software (Dominguez et al., 2003) to generate a model of the eIF1:eIF5-CTD complex (Figure 1G).

In order to validate the eIF1:eIF5-CTD model, we employed a site-directed mutagenesis approach. We examined whether changing the residues on the predicted eIF5-CTD surface would abrogate binding between eIF1 and eIF5. Based on our model (Figure 1G), we created a quadruple mutant eIF5-CTD (eIF5-CTD-Quad; H305D/N306D/E347K/E348K), which remained folded upon incorporation of the four point mutations (Figure S1B). The eIF5-CTD-Quad mutant disrupts the binding of eIF5-CTD to wild-type eIF1, as shown by NMR chemical shift perturbation (Figure S1B&D; right panels). A panel of eIF5-CTD double mutants (H305A/N306A, H305D/N306D, E347A/E348A and E347K/E348K) also maintained their folded state as assessed by NMR (Figure S3A). We examined whether double mutations on the surface of eIF5-CTD affect eIF1 binding; however, we were not able to completely abrogate binding between human eIF1 and eIF5-CTD using any of these double mutations as detected by NMR (Figure S3B). These mutagenesis results are congruent with the model in Figure 1G.

The unstructured N-terminal lysine-rich tail of eIF2β binds eIF5-CTD at an epitope overlapped with the eIF1-binding site

eIF2β-NTD contains three stretches of lysines, named K1, K2 and K3 boxes (Figure 1A and S4A-E). A previous study employing a panel of human eIF2β mutant constructs clearly shows that the NTD of eIF2β is responsible for binding to ^{32}P-labeled rat eIF5 used as a probe, wherein the K2 box of eIF2β was identified as the primary region for binding eIF5 (Das et al., 1997). Based on this finding, we used an eIF2β-NTD construct, which we named eIF2β-K2K3 (eIF2β residues 53-135; which contains the K2-K3 boxes), and we mapped its binding surface on heIF5-CTD (Figure 1A and 2A-B). Unlabeled eIF2β-K2K3 caused chemical shift perturbation and peak broadening of ^{15}N-labeled eIF5-CTD residues (Figure 2CD). We noticed that the region of eIF5-CTD affected by eIF2β-K2K3 binding overlaps the region affected by eIF1 (Compare Figure 1B & 2A). The eIF5-CTD-Quad mutant exhibited a drastically reduced ability to bind eIF2β-K2K3, as evidenced by significantly smaller chemical shift perturbations and less broadening than observed with eIF5-CTD-WT (Compare Figure 2, D & E).

Using isothermal titration calorimetry (ITC), we measured an equilibrium dissociation constant (K_D) for the eIF5-CTD:eIF2β-NTD interaction of ~ 17 μM (Figure S4F). The K_D for the eIF5-CTD interaction with the shorter eIF2β-K2K3 construct was measured as ~4 μM (Figure 3A). The similar eIF5-CTD binding affinities with eIF2β-NTD and eIF2β-K2K3 confirm the findings in a previous eIF2β:eIF5 interaction study (Das et al., 1997) and validates our decision to utilize the eIF2β-K2K3 construct for mapping its interaction with eIF5-CTD. A noticeable baseline deviation after saturation (Figure 3A-B) does not contribute significantly to the qualitative comparisons among differing eIF5-CTD complexes. We found that the eIF5-CTD-DD-mutant:eIF2β-K2K3 interaction exhibits a similar affinity, also in the low μM range with a K_D of ~8 μM (Figure 3B). In contrast, the binding affinity of eIF2β-K2K3 with either eIF5-CTD-KK or eIF5-CTD-Quad was abolished and could not be determined by ITC (Data not shown), hence validating our NMR-chemical shift mapping data and substantiating the identification of a critical linkage between eIF5 and eIF2β.

SAXS reconstitution assay shows that eIF5-CTD does not simultaneously bind eIF2β and eIF1

Since the eIF1:eIF5-CTD interaction could not be quantified by ITC measurements (data not shown), we employed small-angle X-ray scattering (SAXS). In this SAXS reconstitution assay, increasing amounts of eIF1 were titrated into a fixed concentration of eIF5-CTD, and the mixture at each point was subjected to X-ray analysis. The radius of gyration (R_g), being analogous to the moment of inertia in mechanics, reflects the conformational/binding state of the proteins in solution, free or in complex with each other. Increasing the eIF1:eIF5-CTD ratio results in a steady increase in the Rg, consistent with complex formation between eIF1 and eIF5-CTD (Figure 3C; black spheres and Figure S5A). However, there is no saturation of the Rg value, indicative of a weak-binding interaction between eIF1 and eIF5-CTD.

Since eIF1 and eIF2β-NTD bind to overlapping surfaces on eIF5-CTD, we used the SAXS reconstitution assay to monitor whether these three proteins bind simultaneously to form a higher-order complex in solution. Upon the titration of eIF1 to a preformed eIF5-CTD:eIF2β-NTD complex these three proteins do not form a higher-order complex as evidenced by the lack of an increase in the radius of gyration (R_g) (Figure 3C; grey spheres and Figure S5B). The protein ratios in Figure 3D are the same as in Figure 3C, wherein the increase in the number of scatterers (amount of proteins) is related to the linear increase in the SAXS intensity (I/0) (Figure 3D; black and grey spheres).

The interaction between eIF1 and eIF5-CTD is evolutionarily conserved

Upon deletion of the flexible NTT of eIF1, the body of eIF1 still makes contact with eIF5-CTD near residues H305 and N306; other residues showing effects include D344, E348, (in the turn between helices 6 and 7), Y362 (in the turn between helices 7 and 8), and E386 (in the long loop between helices 8 and 9) (Figure S5C-D). Thus, the NTT of human eIF1 plays an ancillary role in binding to eIF5. As previously mentioned, the eIF1 binding surface on eIF5-CTD maps to an overlapping surface wherein eIF2β also binds (Figure S5E), and the mutated Quad residues directly impact this overlapping region (Figure S5F). We proceeded to examine heterologous interactions by NMR spectroscopy, and found that human eIF5-CTD is able to bind to yeast eIF1, while the Quad mutation in human eIF5-CTD abolishes binding to yeast eIF1 (Figure S6A & B, middle and right panels). Importantly, the mapped contact surface on human eIF1 overlaps the previously mapped binding surface on yeast eIF1 for yeast eIF5-CTD (Figure S6C&D) (Reibarkh et al., 2008), involving three conserved human eIF1 residues, F13, A14 and G101 (corresponding to yeast F12, A13 and G97) (Figure S6C vs. D). Figure S6E shows the sequences of human and yeast eIF1 with residues experiencing chemical shift perturbation upon interacting with human and yeast eIF5-CTD, respectively. Interestingly, the yeast *sui1-93-97* mutant exhibits a Sui⁻ phenotype with a well-defined mechanism, involving accelerated eIF1 release from PICs (Cheung et al., 2007).

The Quad mutation impairs eIF5's ability to recruit eIF2-TC to PICs *in vitro*

Previously, we identified eIF5's antagonistic interplay with eIF1 and eIF2-TC within PICs (Nanda et al., 2009). The binding of eIF1 and eIF1A to the 40S subunit promotes its open conformation, favorable for direct tRNA$_i^{Met}$ and mRNA binding to the decoding site (Passmore et al., 2007). In the presence of WT eIF1A, the yeast eIF1-G107K mutant protein diminished stable eIF2-TC loading on 40S subunits *in vitro* (without destabilizing mutant eIF1-G107K binding to the 40S) (Nanda et al., 2009). In this experimental situation (without mRNA), eIF2-TC loading on the 40S is contingent upon a shift to the closed conformation of the PIC, stabilizing tRNA$_i^{Met}$ bound to the P-site. eIF1 antagonizes this shift, and the eIF1-G107K mutant exhibits a stronger antagonistic ability due to its tighter binding to the

40S ribosomal subunit. Interestingly, this effect was overcome by the addition of yeast eIF5 (Nanda et al., 2009). Thus, eIF5 enhances eIF2-TC loading by promoting eIF1 release, which is consistent with our identification of conserved overlapping surfaces for eIF2β-K-boxes and eIF1 in eIF5-CTD, along with our data establishing that human eIF5-CTD does not bind simultaneously to eIF1 and eIF2β-NTD in solution.

In this *in vitro* yeast system, we interpret the ability of the wild-type yeast eIF5 to enhance eIF2-TC binding to the PIC as a measure of its ability to promote eIF1 release. The Quad mutation introduced into the corresponding homologous eIF1/eIF2β-binding surface of yeast eIF5 reduces this eIF5-dependent rescue of eIF2-TC loading in reactions containing eIF1-G107K (Figure 4A). The yeast eIF5-Quad mutant exhibits significantly reduced ability to promote stable eIF2-TC recruitment relative to the WT factor, as evidenced by a 5-fold increase in the concentration of eIF5-Quad mutant required to achieve half maximal eIF2-TC binding (Figure 4A; black curve, eIF5-Quad $K_d = 0.55 \pm 0.1$ µM as compared to the red curve, eIF5-WT $K_d = 0.10 \pm 0.05$ µM). Thus, the diminished ability of eIF5-Quad to enhance observable eIF2-TC loading *in vitro* is likely due to its impaired ability to promote the release of the eIF1-G107K mutant, which is bound tighter than eIF1-WT to 40S ribosomes.

The eIF5-Quad mutant destabilizes the closed state of the PIC *in vitro*

We proceeded to examine whether the Quad residues of eIF5 regulate the conformational change in the PIC response to AUG selection. Previous studies indicated that eIF1A dissociates more slowly from the PIC at AUG versus non-AUG codon (e. g. UUG) (Fekete et al., 2007; Maag et al., 2006). The *in vitro* eIF1A dissociation assay serves as a proxy for monitoring the opening/closing of the PIC upon start codon recognition. Stabilization of eIF1A binding upon start codon recognition is thought to indicate a closed state of the PIC, characterized by a reduced rate of eIF1A dissociation from the PIC *in vitro*, although the physiologically relevant dissociation of eIF1A takes place at the end of the initiation cycle, after subunit joining (Acker et al., 2006). 43S•mRNA(AUG) or 43S•mRNA(UUG) complexes were assembled with eIF1A that was labeled at its C-terminus with fluorescein, in the presence of either eIF5-WT or eIF5-Quad mutant. These labeled complexes were then chased with excess unlabeled eIF1A and dissociation of eIF1A (fluorescently-labeled) was measured over time as a decrease in fluorescence anisotropy. Using eIF5-WT, eIF1A dissociates with biphasic kinetics, with rate constants for the fast and slow phases designated k_1 and k_2, respectively (Fekete et al., 2007; Maag et al., 2006). Previous studies indicated that the slow phase corresponds to eIF1A dissociation from PICs in the closed state, whereas the fast phase represents dissociation from complexes in the open state. K_{amp} is the ratio of the amplitudes of the slow to fast kinetic phases (an apparent equilibrium constant between the two states); hence values of $K_{amp}>1$ indicate that the closed complex predominates in this system.

It was shown previously that the enhancement of eIF1A binding to PICs upon start codon recognition does not happen in the absence of eIF5 (Maag et al., 2006). Consistent with previous studies (Fekete et al., 2007; Maag et al., 2006), the kinetics of eIF1A dissociation from AUG complexes in the presence of eIF5-WT is dominated by the slow phase ($K_{amp} = 6.1 \pm 1.5$; Table I, AUG; row 3) (Figure 4B; red line), whereas replacing AUG with UUG in the model mRNA reduces K_{amp} several fold (to 2.5 ± 0.5), indicating a stabilization of the open state relative to the closed state (Figure 4B; black line). This indicates that eIF5 promotes the shift to the closed state preferentially in response to AUG versus UUG. Dissociation of eIF1A from AUG complexes containing the eIF5-Quad mutant showed a 4-fold reduction in K_{amp} (Table I, AUG, $K_{amp} = 1.5 \pm 0.5$), such that the rapid phase is increased in this reaction (Figure 4B; dark-blue line). For the corresponding UUG complexes, K_{amp} remains low and k_1 and k_2 both are strongly increased by the Quad

substitution (Table I, Quad mutant; UUG $K_{amp} = 1.2 \pm 0.2$) (Figure 4B; light blue line), indicating that the Quad mutation should not confer the ability to initiate from the UUG codon. The Quad mutant's role as a GAP remains intact as evidenced by the ability to induce GTP hydrolysis similar to eIF5-WT (Figure 4C). Therefore, we conclude that the eIF5-Quad mutant destabilizes the closed state of the PIC relative to the open state, without affecting the GAP function. These findings led us to predict that the eIF5-Quad mutation will reduce the ability to access the closed conformation inappropriately at UUG codons in Sui⁻ mutants, thereby conferring an Ssu⁻ phenotype in yeast. This turns out to be the case, as described below.

eIF2β:eIF5-CTD interaction is critical for human eIF5 to complement yeast eIF5 deletion *in vivo*

We turned our attention to the *in vivo* function of the eIF5-CTD interaction network and assessed whether the mutations in the CTD exhibit a phenotype consistent with our biochemical and biophysical data. We employed an *in vivo* assay that exploits the ability of human eIF5 to provide the essential function of yeast eIF5 (Tif5). It was shown previously that mammalian eIF5 manifests the capability to functionally substitute for yeast eIF5 in a yeast strain deleted for the chromosomal gene encoding eIF5 (*tif5Δ*) (Maiti and Maitra, 1997). Here, we introduced into yeast the cloned coding sequences for either human eIF5-WT or the -DD, -KK or -Quad mutants, tagged with the FLAG epitope and placed under the native *TIF5* promoter on a *LEU2* single-copy (sc) plasmid, and confirmed equal expression of eIF5-WT and mutant forms by Western analysis (Figure 5A, bottom two gels). The plasmids were then tested for the ability to replace a sc *URA3 TIF5* plasmid in a *tif5Δ* strain using the drug 5-fluoro-orotic acid (5FOA) to select against *URA3* (plasmid-shuffling). The plasmid encoding FLAG-tagged human eIF5 harboring the DD substitutions (heIF5-DD-FLAG) complemented *tif5Δ* similar to those encoding human eIF5-WT untagged or FLAG-tagged (Figure 5A; rows 1-3). By contrast, the constructs encoding the KK or Quad variants of FLAG-tagged heIF5 did not complement *tif5Δ* (Figure 5A; rows 4-5). Thus, the KK or Quad substitutions, but not the DD substitutions, abolish the ability of human eIF5 to provide the essential function of eIF5 in yeast cells. Because the Quad mutation is required to disrupt binding of human eIF5-CTD to eIF1 (Figures S1E & S3B), whereas both the KK and Quad mutations abolish eIF5-CTD binding to eIF2β-NTD, hence we conclude that the essential partner of human eIF5-CTD in yeast cells is likely to be eIF2β-NTD.

The KK and Quad mutations in yeast eIF5-CTD reduce aberrant initiation from a UUG start codon *in vivo*

We proceeded to evaluate the effects of introducing the DD, KK or Quad mutations into yeast *TIF5* gene on the accuracy of start codon selection *in vivo*. To this end, we constructed these *TIF5* mutants in the *tif5Δ* strain harboring the *his4-306* allele of the *HIS4* gene in which the AUG start codon is altered and translation begins on a downstream UUG codon. The strain containing WT *TIF5-FL* cannot grow on medium devoid of histidine (Figure 5B, row 1, −His medium) because the start codon mutation in *his4-306* abolishes expression of this histidine biosynthetic enzyme. A strain containing *TIF5-G58S* altering the eIF5-NTD can grow on −His medium (His⁺ phenotype) because an in-frame UUG triplet at the third codon of *his4-306* can be used as the initiation codon in cells harboring this eIF5 Sui⁻ mutation (Singh et al., 2005) (Figure 5B, row 2). The strain harboring *TIF5-Quad* did not display a slow growth phenotype on +His medium (Figure 5B; row 3, +His) nor a His⁺/Sui⁻ phenotype on −His medium (Figure 5B; row 3, −His). The absence of a Sui⁻ phenotype (Sui⁺) for the *TIF5-Quad* mutant is consistent with our *in vitro* analysis of eIF1A dissociation kinetics, which revealed a predominantly open state of 43S.UUG complexes harboring the yeast eIF5-Quad mutant (Figure 4B and Table 1).

As noted above, the analysis of eIF1A dissociation kinetics led us to predict that the *TIF5-Quad* mutant would display an Ssu⁻ phenotype, suppressing the relaxed stringency of start codon recognition conferred by a Sui⁻ mutation. To test this prediction, we asked whether the *TIF5-Quad* mutation can suppress the dominant His⁺/Sui⁻ phenotype conferred by the *SUI3-2* mutation in eIF2β (S264Y substitution), which appears to result from elevated eIF5-independent GTPase activity by the eIF2-TC and a weakened interaction between Met-tRNA$_i^{Met}$ and eIF2-GTP (Huang et al., 1997). As expected, introducing plasmid-borne *SUI3-2,* but not WT *SUI3,* into the *his4-306* strain harboring WT *TIF5* confers growth on the –His medium (Figure 5C; rows 1-2, –His). Furthermore, the dominant His⁺/Sui⁻ phenotype of *SUI3-2* is partially suppressed in the strain harboring a known Ssu⁻ allele of *TIF5, tif5-G62S* (Asano et al., 2001), as only weak growth occurred on –His medium even after 5 days of incubation (Figure 5C; compare row 9 to row 1, –His). In agreement with our prediction, the *TIF5-Quad* allele confers an Ssu⁻ phenotype nearly as strong as that of *tif5-G62S* (Figure 5C; compare rows 1, 7 and 9, –His). Importantly, the *tif5-KK* allele also confers a marked Ssu⁻ phenotype, only slightly less than that of *tif5-Quad*, whereas the *tif5-DD* allele displays little or no Ssu⁻ phenotype (Figure 5C; rows 3, 5 and 7; –His). The fact that the *TIF5-KK* mutation confers an obvious Ssu⁻ phenotype suggests that the weakened binding of eIF5-CTD to eIF2β produced by the KK substitution is responsible for this phenotype. These findings provide strong support for the conclusion that disrupting the interaction of eIF5-CTD with eIF2β destabilizes the closed conformation of the PIC, increasing the stringency of start codon recognition and thus decreasing initiation at near-cognate UUG codons *in vivo*.

In vivo evidence that the KK and Quad substitutions in eIF5-CTD confer Ssu⁻ phenotypes by decreasing eIF1 release from the PIC

Our biochemical analysis of the eIF5-Quad mutant showed a reduction in eIF2-TC recruitment to PICs, which is indicative of a defect in promoting eIF1 dissociation upon AUG recognition. The previously described G107R and G107K eIF1 mutants exhibit the same defect in eIF2-TC recruitment. The G107R/K substitutions increase the UUG:AUG ratio (Sui⁻ phenotype) primarily by decreasing initiation at AUG rather than elevating UUG initiation (Nanda et al., 2009). By contrast, other eIF1 mutations, notably the 93-97 substitution in helix α2 (Cheung et al., 2007), appear to increase the UUG:AUG ratio by provoking more rapid dissociation at UUG codons owing to weaker eIF1 binding to the PIC. Accelerated eIF1 release likely also explains the Sui⁻ phenotype of s*ui1-K60E* (Martin-Marcos et al., 2011), since Lys-60 contacts 18S rRNA in the eIF1:40S crystal structure (Rabl et al., 2011) and overexpression of *sui1-K60E* suppresses its Sui⁻ phenotype in the manner observed previously for *sui1-93-97* (data not shown). Because the Quad substitution impairs eIF1 dissociation, we reasoned that it should not suppress the elevated UUG:AUG ratio conferred by the G107R/K substitutions because they also impede eIF1 dissociation, but that it should suppress the Sui⁻ phenotypes of the 93-97 and K60E substitutions by mitigating the accelerated eIF1 dissociation they engender.

We tested these predictions by examining a set of *sui1Δ his4-301* yeast strains (with a different start codon mutation at *HIS4*) containing plasmid-borne *TIF5* and *SUI1* alleles encoding the eIF5 and eIF1 mutants of interest and the chromosomal *TIF5* allele placed under the *GAL1* promoter to enable its repression on glucose medium. As expected, the WT *TIF5* strain expressing eIF1-93-97 has a slow-growth (Slg⁻) phenotype at 37°C on +His (glucose) medium but can grow on media containing no histidine, indicating the Sui⁻ phenotype (Cheung et al., 2007). Interestingly, the *TIF5-KK* and *TIF5-Quad* alleles improve the growth of *sui1-93-97* cells on +His medium, but diminish their growth on –His medium; whereas the *TIF5-DD* allele only reduces growth on –His (Figure 6A). These results suggest that the *KK* and *Quad* mutations suppress the Sui⁻ phenotype of *sui1-93-97* cells more

effectively than does *TIF5-DD*. Supporting this, the *KK* and *Quad* mutations exceed *DD* in decreasing the UUG:AUG initiation ratio in *sui1-93-97* cells measured using *HIS4-lacZ* fusions with an AUG or UUG start codon. Thus, the *KK* and *Quad* mutations reduce the UUG:AUG ratio by ≈40%, similar in magnitude to reductions observed for Ssu⁻ substitutions in eIF1A (Saini et al., 2010), whereas the *DD* mutation produces only a ≈20% reduction in the ratio. Importantly, the *KK* and *Quad* mutations also exceed the *DD* mutation in reducing the His⁺/Sui⁻ phenotype and elevated UUG:AUG ratio in *sui1-K60E* cells (Figure S7A-B).

The G107R substitution in eIF1 increases the UUG:AUG ratio to the same extent as does the 93-97 substitution (compare Figures 6B and 6D). Importantly, however, none of the CTD mutations of eIF5 produces a significant reduction in this ratio (Figure 6D). In addition, the *KK* and *Quad* mutations exacerbate the Slg⁻ phenotype of *sui1-G107R* cells (Figure 6C), opposite the effect displayed in *sui1-93-97* cells, and similar findings were observed for the mechanistically related G107K mutation (Figures S7C-D). These findings support our prediction that the *KK* and *Quad* substitutions would not suppress the elevated UUG:AUG initiation ratio, and would intensify the defect in eIF1 release on AUG recognition, conferred by eIF1-G107R/K. These results provide *in vivo* evidence that the *KK* and *Quad* substitutions impair the eIF5-CTD function in releasing eIF1 from the closed complex upon start codon recognition. Our molecular interpretations of the Ssu⁻ and Slg-phenotypes of the various mutants harboring the eIF5-CTD mutations are shown in Tables S2 and S3, respectively.

DISCUSSION

eIF1 binds in the vicinity of the P site on the 40S subunit and contacts Met-tRNA$_i^{Met}$ (Lomakin et al., 2003; Rabl et al., 2011). Therefore, we sought to use the eIF1:eIF5-CTD model to infer the position of eIF5-CTD in the PIC, by superimposing the eIF1:eIF5-CTD complex onto the eIF1:40S structure (Rabl et al., 2011) by aligning the common component: eIF1 (Figure 7A-B). The resulting model places eIF5-CTD in the vicinity of the Met-tRNA$_i^{Met}$, consistent with the eIF5-NTD binding to eIF2γ near the 3′ end of the tRNA (Alone and Dever, 2006; Conte et al., 2006).

The conclusion that the CTD of eIF5 promotes eIF1 dissociation is supported by our findings that the Quad substitution impairs the ability of eIF5, when added in excess, to reverse the antagonistic effect of eIF1-G107K on eIF2-TC binding in the reconstituted system. The novel mechanism wherein overlapping surfaces on the CTD of eIF5 are utilized to promote eIF1 dissociation was not known and could not have been predicted by previous experiments. We provide biochemical evidence that the CTD of eIF5 plays a previously unknown role in the promotion of eIF1 dissociation upon AUG recognition via its dynamic interaction with eIF1 and eIF2β, which is based on the following two findings: 1) The Quad substitution impairs eIF5's ability to promote stable recruitment of eIF2-TC to PICs containing eIF1-G107K (which binds with greater affinity to 40S ribosomes) without mRNA *in vitro*. 2) The Quad substitution destabilizes closed PIC conformation with mRNAs upon start codon recognition. It is important to note that the role of eIF5-CTD in promoting eIF1 release is independent of the eIF5 GAP function catalyzed by the NTD.

A key question is whether the newly identified function of the CTD of eIF5 in promoting eIF1 release involves both of its interactions with eIF1 and eIF2β. We show here that the KK substitution on the CTD of eIF5 is sufficient to drastically reduce its binding to eIF2β but not to eIF1. Thus, it can be deduced that disrupting the interaction of eIF5-CTD with eIF2β is likely to be responsible for destabilizing the closed PIC conformation and conferring the Ssu⁻ phenotypes displayed by the *eIF5-KK* and *eIF5-Quad* mutations. In fact,

it was shown previously that elimination of K-boxes 1 and 2 from eIF2β also confers a Ssu⁻ phenotype (Laurino et al., 1999). Hence, it seems likely that the Ssu⁻ phenotypes produced by these newly identified substitutions in the CTD of eIF5 (along with the previously identified eIF2β-NTD Ssu⁻ phenotype), directly impact the linkage of eIF2β with eIF5 within the PIC.

It is plausible that the eIF1:eIF5-CTD complex is stabilized by the mutual interaction of these factors with eIF3c, which was demonstrated *in vitro* for the cognate yeast proteins (Asano et al., 2000). We propose that the eIF1:eIF5-CTD interaction is redundant with other interactions that stabilize eIF1 binding to the 40S leading to an open PIC conformation, hence eliminating this interaction is probably not sufficient to accelerate eIF1 dissociation at UUG codons *in vivo*. Our conclusion that eIF5-CTD stabilizes the closed conformation of PICs upon start codon recognition via its interaction with eIF1 and eIF2β was based on the cumulative breadth of data ranging from NMR spectroscopy, ITC, SAXS and *in vitro* yeast reconstituted system. The *in vitro* assays employed in this study, which include eIF1, eIF1A, eIF2-TC, eIF5 and 40S ribosomes (with and without mRNA), utilize the basic components for start codon recognition and have been consistently implemented as useful tools to decipher biochemical events surrounding start codon recognition (Maag et al., 2006; Nanda et al., 2009). Based on our *in vitro* assays, we propose that eIF5 interactions, particularly with its CTD, are sufficient to promote eIF1 release by stabilizing the closed complex via its interaction with eIF2β. Our hypothesis was further examined using *in vivo* experiments, wherein we dissect the cause of Ssu-phenotypes produced by mutations in the CTD of eIF5. We show that the *KK* and *Quad* mutants exhibit strong Ssu⁻ phenotypes, which further substantiates the novel role of eIF5-CTD in facilitating the stabilization of the closed state of PICs upon start codon recognition via its dynamic interplay with eIF1 and eIF2β.

The common interface on eIF5-CTD that contacts eIF2β also interacts with eIF1, in a manner disrupted by the Quad substitution. eIF1 and eIF2β do not form a higher-order complex with eIF5-CTD in our SAXS reconstitution assay, hence an intriguing model would be that eIF5-CTD first interacts with eIF1 in the open, scanning conformation of the PIC and then switches partners to interact with eIF2β in the closed conformation upon AUG recognition (Figure 7C). In this view, the interaction network (including eIF5-CTD) positions eIF1 in the decoding site and mediates scanning. Upon start codon selection, we propose the following possible model of events surrounding start codon recognition. eIF5-CTD binds to eIF2β, which in turn favors the release of eIF1 from the PIC and essentially puts an end to the ribosomal scanning mechanism. This would also impede eIF1's re-association with the 40S and drive the conformational rearrangement of the PIC to the closed state.

The hypothesis that the disruption of the eIF1:eIF5-CTD interaction by eIF2β triggers the critical shift from the open state (scanning-competent) to the closed state (scanning-incompetent) led us to conclude that the CTD of eIF5 stabilizes the closed state of the PIC in which eIF1 is no longer bound (Figure 7C). This model is fully consistent with our biophysical, biochemical and genetic data wherein we strategically disrupt the eIF5-CTD:eIF2β interaction that destabilizes the closed state of the complex and prevents eIF5-CTD from promoting eIF1 release. We do note that *in vivo* other initiation factors, e.g. possibly eIF1A, eIF3 or eIF4G, could also play contributing roles in the observed Ssu⁻ phenotype caused by mutations in the CTD of eIF5. This study opens a new avenue for further investigations to continue deciphering the effect of eIF5-CTD's interaction with its cognate partners, and its crucial role in mediating the closure of PICs upon start codon recognition.

EXPERIMENTAL PROCEDURES

Biophysical experiments and analyses (NMR, SAXS and ITC)

NMR experiments were performed as described previously (Marintchev et al., 2007) and written in more detail in the Supplemental Information. We recorded a set of triple resonance experiments needed for backbone assignments of human eIF5-CTD. Assignments were completed for 95% of the residues in the human eIF5-CTD, using standard techniques and IBIS (Hyberts and Wagner, 2003). Chemical shift mapping was done as previously described (Marintchev et al., 2007). A paramagnetic spin label strategy was used to obtain intermolecular distance restraints between human eIF1 and eIF5-CTD (Battiste and Wagner, 2000).

SAXS and ITC experiments are also described in more detail in the Supplemental Information. SAXS of eIF5, eIF1:eIF5-CTD, eIF1:(eIF5-CTD+eIF2β-NTD) were measured in 20 mM Tris.HCl, pH 7.4, 200 mM NaCl, 0.5 mM TCEP, and eIF5-CTD at a final concentration of 90 μM, while eIF1 concentrations were in the range from 90μM to 1,800 μM. Protein samples for ITC experiments were prepared in 20 mM Tris.HCl pH 7.2, 200 mM NaCl, 0.5 mM TCEP, 0.5 mM EDTA. A Microcal ITC$_{200}$ calorimeter was run at an equilibrium temperature of 25°C. The concentration of the protein in the well was roughly 10 times the estimated K_D and the concentration of the protein in the syringe was seven times the one in the well.

Yeast biochemistry and genetics experiments

Yeast biochemistry experiments were performed as described previously (Maag et al., 2006; Nanda et al., 2009). eIF2-TC recruitment to 43S PICs experiments were carried out with a native gel assay as previously described (Acker et al., 2007). Unlabeled eIF1A was added to preassembled 43S·mRNA complexes (containing eIF1A-FL; flourescently-labeled) and anisotropy values were plotted as a function of time (Maag et al., 2006). GTP hydrolysis experiments were performed as described previously (Algire et al., 2005). Yeast genetics experiments were performed as described previously (Cheung et al., 2007; Nanda et al., 2009; Reibarkh et al., 2008; Yamamoto et al., 2005). These experiments were written in more detail in the Supplemental Information.

Supplementary Material

Refer to Web version on PubMed Central for supplementary material.

Acknowledgments

REFERENCES

Acker MG, Kolitz SE, Mitchell SF, Nanda JS, Lorsch JR. Reconstitution of yeast translation initiation. Methods Enzymol. 2007; 430:111–145. [PubMed: 17913637]

Acker MG, Shin BS, Dever TE, Lorsch JR. Interaction between eukaryotic initiation factors 1A and 5B is required for efficient ribosomal subunit joining. J Biol Chem. 2006; 281:8469–8475. [PubMed: 16461768]

Algire MA, Maag D, Lorsch JR. Pi release from eIF2, not GTP hydrolysis, is the step controlled by start-site selection during eukaryotic translation initiation. Mol Cell. 2005; 20:251–262. [PubMed: 16246727]

Alone PV, Dever TE. Direct binding of translation initiation factor eIF2gamma-G domain to its GTPase-activating and GDP-GTP exchange factors eIF5 and eIF2B epsilon. J Biol Chem. 2006; 281:12636–12644. [PubMed: 16522633]

Asano K, Clayton J, Shalev A, Hinnebusch AG. A multifactor complex of eukaryotic initiation factors, eIF1, eIF2, eIF3, eIF5, and initiator tRNA(Met) is an important translation initiation intermediate in vivo. Genes Dev. 2000; 14:2534–2546. [PubMed: 11018020]

Asano K, Sachs MS. Translation factor control of ribosome conformation during start codon selection. Genes & development. 2007; 21:1280–1287. [PubMed: 17545463]

Asano K, Shalev A, Phan L, Nielsen K, Clayton J, Valasek L, Donahue TF, Hinnebusch AG. Multiple roles for the C-terminal domain of eIF5 in translation initiation complex assembly and GTPase activation. Embo J. 2001; 20:2326–2337. [PubMed: 11331597]

Battiste JL, Wagner G. Utilization of site-directed spin labeling and high-resolution heteronuclear nuclear magnetic resonance for global fold determination of large proteins with limited nuclear overhauser effect data. Biochemistry. 2000; 39:5355–5365. [PubMed: 10820006]

Cheung YN, Maag D, Mitchell SF, Fekete CA, Algire MA, Takacs JE, Shirokikh N, Pestova T, Lorsch JR, Hinnebusch AG. Dissociation of eIF1 from the 40S ribosomal subunit is a key step in start codon selection in vivo. Genes Dev. 2007; 21:1217–1230. [PubMed: 17504939]

Conte MR, Kelly G, Babon J, Sanfelice D, Youell J, Smerdon SJ, Proud CG. Structure of the eukaryotic initiation factor (eIF) 5 reveals a fold common to several translation factors. Biochemistry. 2006; 45:4550–4558. [PubMed: 16584190]

Das S, Maiti T, Das K, Maitra U. Specific interaction of eukaryotic translation initiation factor 5 (eIF5) with the beta-subunit of eIF2. J Biol Chem. 1997; 272:31712–31718. [PubMed: 9395514]

Dominguez C, Boelens R, Bonvin AM. HADDOCK: a protein-protein docking approach based on biochemical or biophysical information. J Am Chem Soc. 2003; 125:1731–1737. [PubMed: 12580598]

Fekete CA, Mitchell SF, Cherkasova VA, Applefield D, Algire MA, Maag D, Saini AK, Lorsch JR, Hinnebusch AG. N- and C-terminal residues of eIF1A have opposing effects on the fidelity of start codon selection. Embo J. 2007; 26:1602–1614. [PubMed: 17332751]

Fletcher CM, Pestova TV, Hellen CU, Wagner G. Structure and interactions of the translation initiation factor eIF1. Embo J. 1999; 18:2631–2637. [PubMed: 10228174]

Hinnebusch AG. Molecular mechanism of scanning and start codon selection in eukaryotes. Microbiology and molecular biology reviews : MMBR. 2011; 75:434–467. [PubMed: 21885680]

Huang HK, Yoon H, Hannig EM, Donahue TF. GTP hydrolysis controls stringent selection of the AUG start codon during translation initiation in Saccharomyces cerevisiae. Genes Dev. 1997; 11:2396–2413. [PubMed: 9308967]

Hyberts SG, Wagner G. IBIS - a tool for automated sequential assignment of protein spectra from triple resonance experiments. J Biomol NMR. 2003; 26:335–344. [PubMed: 12815260]

Laurino JP, Thompson GM, Pacheco E, Castilho BA. The beta subunit of eukaryotic translation initiation factor 2 binds mRNA through the lysine repeats and a region comprising the C2-C2 motif. Molecular and cellular biology. 1999; 19:173–181. [PubMed: 9858542]

Lomakin IB, Kolupaeva VG, Marintchev A, Wagner G, Pestova TV. Position of eukaryotic initiation factor eIF1 on the 40S ribosomal subunit determined by directed hydroxyl radical probing. Genes Dev. 2003; 17:2786–2797. [PubMed: 14600024]

Maag D, Algire MA, Lorsch JR. Communication between eukaryotic translation initiation factors 5 and 1A within the ribosomal pre-initiation complex plays a role in start site selection. J Mol Biol. 2006; 356:724–737. [PubMed: 16380131]

Maiti T, Maitra U. Characterization of translation initiation factor 5 (eIF5) from Saccharomyces cerevisiae. Functional homology with mammalian eIF5 and the effect of depletion of eIF5 on protein synthesis in vivo and in vitro. J Biol Chem. 1997; 272:18333–18340. [PubMed: 9218474]

Marintchev A, Frueh D, Wagner G. NMR methods for studying protein-protein interactions involved in translation initiation. Methods Enzymol. 2007; 430:283–331. [PubMed: 17913643]

Martin-Marcos P, Cheung YN, Hinnebusch AG. Functional elements in initiation factors 1, 1A and 2{beta} discriminate against poor AUG context and non-AUG start codons. Molecular and cellular biology. 2011

Nanda JS, Cheung YN, Takacs JE, Martin-Marcos P, Saini AK, Hinnebusch AG, Lorsch JR. eIF1 controls multiple steps in start codon recognition during eukaryotic translation initiation. J Mol Biol. 2009; 394:268–285. [PubMed: 19751744]

Passmore LA, Schmeing TM, Maag D, Applefield DJ, Acker MG, Algire MA, Lorsch JR, Ramakrishnan V. The eukaryotic translation initiation factors eIF1 and eIF1A induce an open conformation of the 40S ribosome. Mol Cell. 2007; 26:41–50. [PubMed: 17434125]

Pestova TV, Kolupaeva VG. The roles of individual eukaryotic translation initiation factors in ribosomal scanning and initiation codon selection. Genes Dev. 2002; 16:2906–2922. [PubMed: 12435632]

Pestova TV, Lomakin IB, Lee JH, Choi SK, Dever TE, Hellen CU. The joining of ribosomal subunits in eukaryotes requires eIF5B. Nature. 2000; 403:332–335. [PubMed: 10659855]

Rabl J, Leibundgut M, Ataide SF, Haag A, Ban N. Crystal structure of the eukaryotic 40S ribosomal subunit in complex with initiation factor 1. Science. 2011; 331:730–736. [PubMed: 21205638]

Reibarkh M, Yamamoto Y, Singh CR, del Rio F, Fahmy A, Lee B, Luna RE, Ii M, Wagner G, Asano K. Eukaryotic initiation factor (eIF) 1 carries two distinct eIF5-binding faces important for multifactor assembly and AUG selection. J Biol Chem. 2008; 283:1094–1103. [PubMed: 17974565]

Saini AK, Nanda JS, Lorsch JR, Hinnebusch AG. Regulatory elements in eIF1A control the fidelity of start codon selection by modulating tRNA(i)(Met) binding to the ribosome. Genes Dev. 2010; 24:97–110. [PubMed: 20048003]

Singh CR, Curtis C, Yamamoto Y, Hall NS, Kruse DS, He H, Hannig EM, Asano K. Eukaryotic translation initiation factor 5 is critical for integrity of the scanning preinitiation complex and accurate control of GCN4 translation. Mol Cell Biol. 2005; 25:5480–5491. [PubMed: 15964804]

Sokabe M, Fraser CS, Hershey JW. The human translation initiation multi-factor complex promotes methionyl-tRNAi binding to the 40S ribosomal subunit. Nucleic acids research. 2011

Watanabe R, Murai MJ, Singh CR, Fox S, Ii M, Asano K. The eukaryotic initiation factor (eIF) 4G HEAT domain promotes translation re-initiation in yeast both dependent on and independent of eIF4A mRNA helicase. J Biol Chem. 2010; 285:21922–21933. [PubMed: 20463023]

Yamamoto Y, Singh CR, Marintchev A, Hall NS, Hannig EM, Wagner G, Asano K. The eukaryotic initiation factor (eIF) 5 HEAT domain mediates multifactor assembly and scanning with distinct interfaces to eIF1, eIF2, eIF3, and eIF4G. Proc Natl Acad Sci U S A. 2005; 102:16164–16169. [PubMed: 16254050]

Yu Y, Marintchev A, Kolupaeva VG, Unbehaun A, Veryasova T, Lai SC, Hong P, Wagner G, Hellen CU, Pestova TV. Position of eukaryotic translation initiation factor eIF1A on the 40S ribosomal subunit mapped by directed hydroxyl radical probing. Nucleic Acids Res. 2009; 37:5167–5182. [PubMed: 19561193]

Highlights for Cell Reports-Luna 2012

-- Pinpointing four residues on eIF5-CTD unveils a dynamic interplay with eIF1 and eIF2β

-- eIF5 Quad mutant impairs the ability of PICs to close on start codons *in vitro*

--eIF5-CTD facilitates the shift of PICs from the open to closed conformation *in vivo*

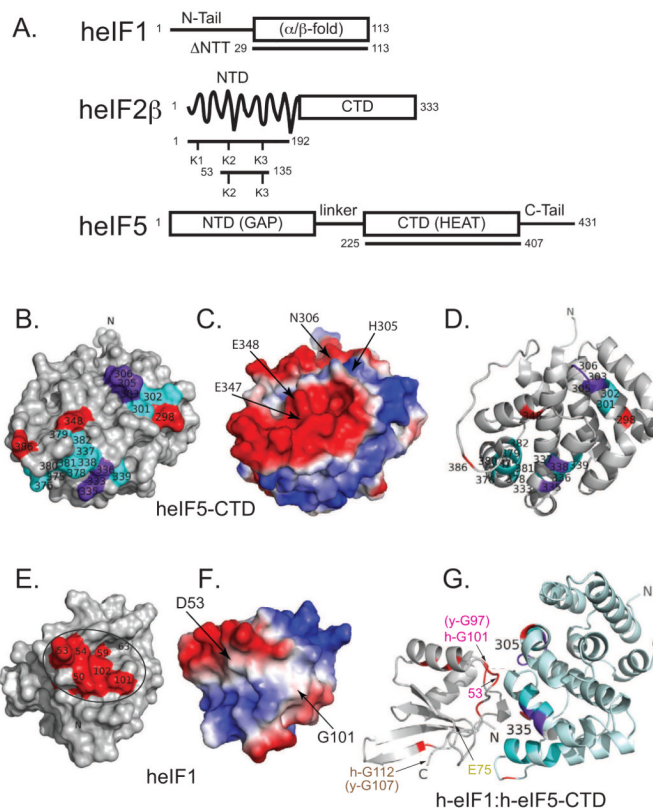--CTD of eIF5 promotes start codon recognition by interacting with eIF1 and eIF2β

Figure 1. eIF5-CTD and the globular domain of eIF1 form a specific but weak binary complex with a well-defined interface

(A) Domain organization of eIF1, eIF2β and eIF5 constructs used in this work. Abbreviations: NTD, amino(N)-terminal domain; NTT, amino(N)-terminal tail; CTD, carboxyl(C)-terminal domain; GAP, GTPase-activating protein; eIF5-CTD is a member of the HEAT domain family, Huntingtin, eukaryotic elongation factor 3 (eEF3), protein phosphatase 2A and TOR1 (target of rapamycin); α/β fold, eIF1 contains two α-helices on one side of a five-stranded parallel and antiparallel β-sheet. (B) NMR mapping of the eIF1 binding surface on eIF5-CTD (1IU1). Contacts are only observed on one face of the domain. eIF5-CTD residues wherein eIF1 causes chemical shift perturbations are painted red, residues that experience resonance broadening in paramagnetic relaxation enhancement (PRE) experiments are painted cyan, and residues affected in both experiments are painted purple. The figure seems to indicate two distinct binding patches based on monitoring backbone signals. As in helical proteins contacts are mainly made by side chains, which are more difficult to follow in chemical shift mapping experiments it is likely that the binding face is contiguous. (C) eIF1 binding surface on eIF5-CTD showing the electrostatic potential of the surface of eIF5-CTD, same orientation as Figure 1B. (D) eIF1 binding surface on eIF5-CTD depicted as a ribbon diagram, similar orientation as Figure 1B adjusted to show electrostatics. (E) eIF5-CTD binding surface on eIF1 (2IF1) is circled. eIF1 residues wherein eIF5-CTD causes chemical shift perturbations are painted red. The unstructured NTT of eIF1 is not shown for clarity. (F) eIF5-CTD binding surface on eIF1 showing the electrostatic potential of the surface of eIF1, similar orientation as Figure 1E but adjusted to show electrostatics. (G) Model for the eIF1:eIF5-CTD complex generated by the HADDOCK software from data summarized in Figure 1B, E and Supplemental Figure 2. The same interface-coloring scheme is used as in B, D, E and G. The location of one of the five single-cysteine mutants, eIF1-E75, is colored yellow. This residue was mutated to a

single cysteine and used to attach a spin-label for paramagnetic relaxation enhancement experiments. Human eIF1-G101 is colored red and it is located within the interaction interface; this residue corresponds to yeast eIF1-G97. The location of human eIF1-G112 is colored brown and it is not located within the interaction interface; this residue corresponds to yeast eIF1-G107.
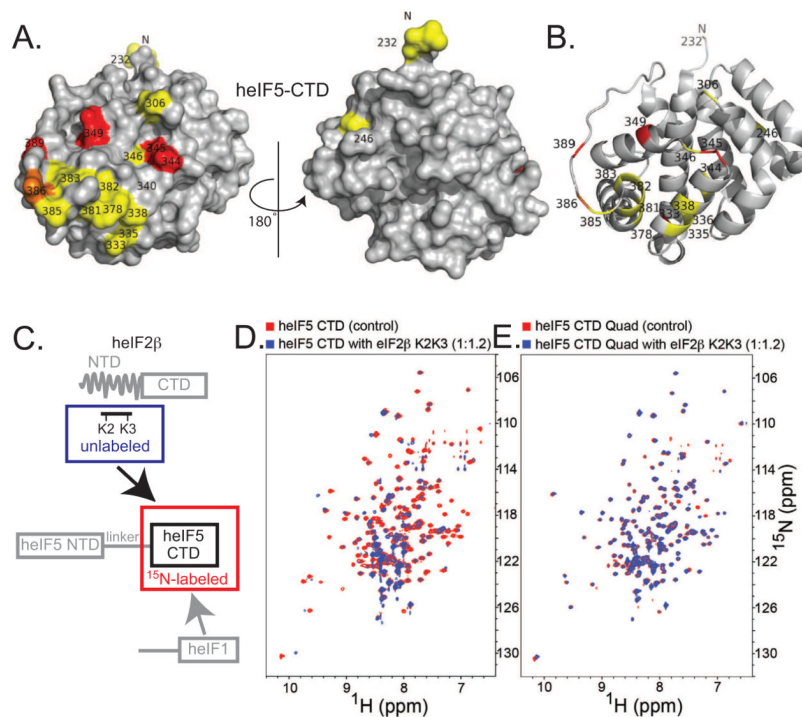
Figure 2. The eIF2β-K2K3 segment contacts eIF5-CTD on a site partially overlapped with the eIF1 binding face

(A) eIF2β-K2K3 binding surface on eIF5-CTD. Two orientations are shown as surface representations; left orientation is the same as Figure 1B. Residues wherein eIF2β-K2K3 causes chemical shift perturbations are painted red, those experiencing line broadening are painted yellow, and those seeing both effects are painted orange. (B) eIF2β-K2K3 binding surface on eIF5-CTD depicted as ribbons, same orientation as left in A. (C) Schematic representation of the labeling scheme used in the proton-nitrogen correlation spectra: 15N-labeled eIF5-CTD is measured alone (residues 225-407) (circumscribed in a red box) and in the presence of unlabeled eIF2β-K2K3 (residues 53-135) (circumscribed in a blue box). (D) Overlay of ^{1}H-^{15}N HSQC spectra of 0.2 mM ^{15}N-labeled wild-type eIF5-CTD domain alone (red) and in the presence of 0.24 mM unlabeled eIF2β-K2K3 (blue). (E) Overlay of ^{1}H-^{15}N HSQC spectra of 0.2 mM ^{15}N-labeled eIF5-CTD-Quad mutant domain alone (red) and in the presence of 0.24 mM unlabeled eIF2β-K2K3 (blue).
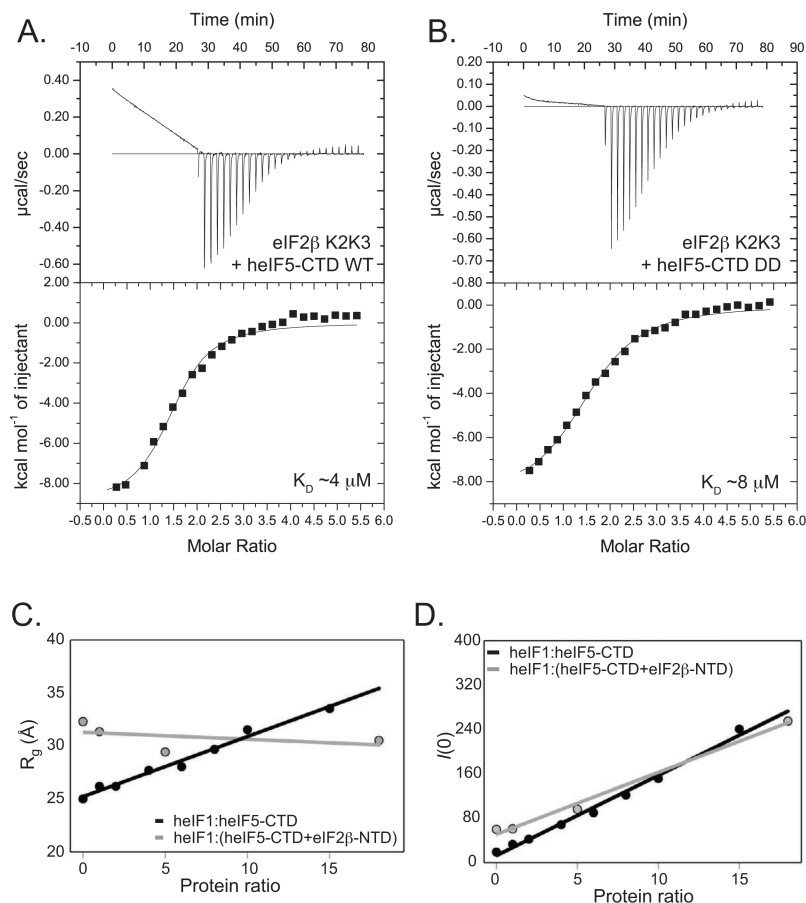
Figure 3. ITC and SAXS narrow down the eIF2β-binding site and suggest competitive binding with eIF1

(A) Isothermal Titration Calorimetry (ITC) analysis of the eIF5-CTD:eIF2β-K2K3 interaction. A solution of eIF2β-K2K3 injected with eIF5-CTD wild-type (WT) (K_D, ~4 µM). (B) ITC analysis of the eIF5-CTD-DD mutant:eIF2β-K2K3 interaction. A solution of eIF2β-K2K3 injected with eIF5-CTD-DD (K_D, ~8 µM). Interestingly, the KK- and/or Quad(DDKK)-mutations of eIF5-CTD abrogate binding to eIF2β. (C&D) SAXS reconstitution assay used to monitor complex formations. Linear relation of the low-angle portion of the data corresponds to well-behaved proteins devoid of aggregation, even in samples with high concentration. (C) SAXS results plotting the radius of gyration (R_g) versus eIF1:eIF5-CTD (black) and eIF1:(eIF5-CTD+eIF2β-NTD) (gray) protein ratios. The data indicate that eIF1 binds eIF5-CTD but does not displace eIF2β-NTD nor form a heterotrimeric complex. (D) Scattering intensities (I/0) shown as a function of concentration dependence, same protein samples as in Figure 3C. Plotting the scattering intensity (Y-axis) versus eIF1:(eIF5-CTD+eIF2β-NTD) molar ratios (X-axis; grey lines) shows a concentration dependence. The same was done for eIF1:eIF5-CTD ratios (black lines). Data were collected for eIF5-CTD (90 µM) titrated with increasing amounts of eIF1. Radius of gyration serves as an indicator for the formation of higher-order protein complexes. SAXS results plotting the radius of gyration (Y-axis) versus protein ratios (X-axis). Black circles, eIF5-CTD domain (90 µM) titrated with increasing amounts of eIF1 (90 µM, 180 µM, 360 µM, 540 µM, 720 µM, 900 µM, 1,350 µM and 1,800 µM). Grey circles, eIF5-CTD:eIF2β-NTD FPLC-purified complex (90 µM) titrated with increasing amounts of eIF1 (90 µM, 450 µM and 1,620 µM).
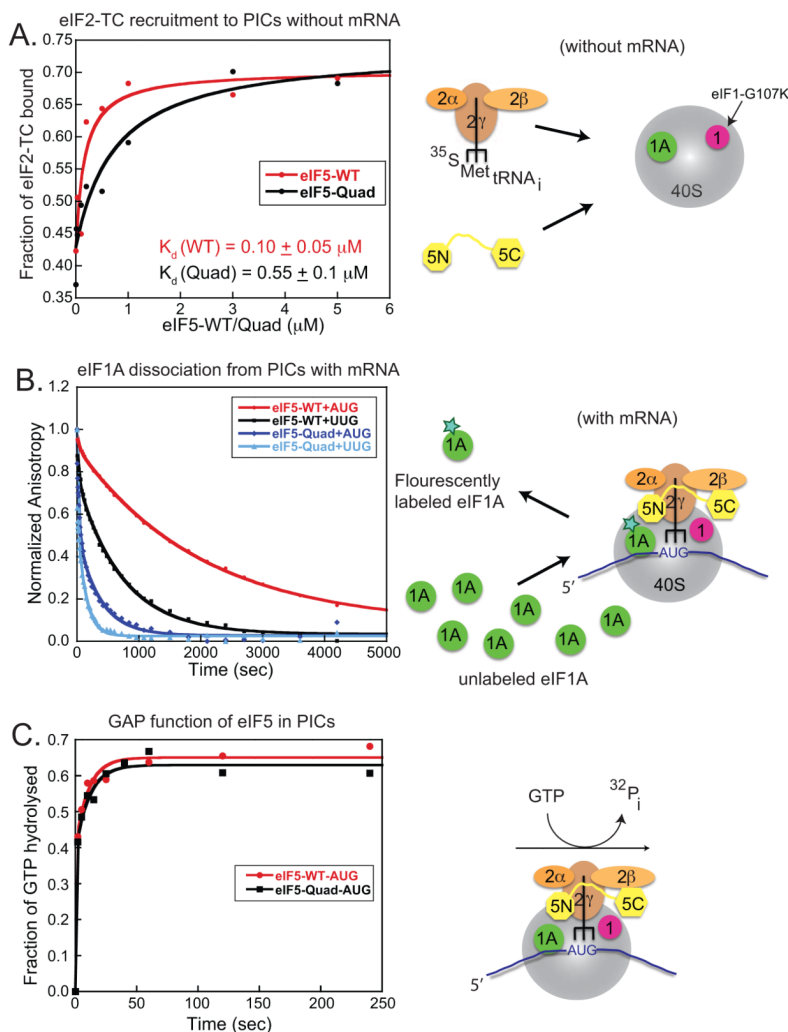
Figure 4. Biochemical evidence that eIF5-CTD functions to promote eIF1 release and the closed complex

These experiments used purified yeast eIFs and ribosomes, as summarized schematically on the right. (A) eIF5-Quad mutant reduces eIF2-TC recruitment to 43S complex (–AUG) *in vitro*. eIF5-Quad mutant is unable to efficiently suppress the eIF2-TC recruitment defect conferred by the G107K eIF1 mutant (corresponds to human eIF1-G112) to the same extent obtained by WT eIF5. In this experiment using yeast eIF1-G107K-mutant and wild-type eIF1A, eIF2-TC binding to 40S is severely compromised but this effect is rescued by adding high amounts of wild-type eIF5 (red curve). A yeast eIF5-Quad mutant (V316D, T317D, S357K, E358K) is not able to rescue the eIF2-TC recruitment defect imposed by eIF1-G107K (black curve). In the case of WT eIF1, eIF5 is not needed for efficient eIF2-TC recruitment under these experimental conditions (data not shown). (B) Effect of the eIF5-Quad mutant on eIF1A dissociation from 43S (AUG)/(UUG) Complexes. The eIF5-Quad mutant destabilizes 43S (AUG)/(UUG) complexes, which leads to eIF1A dissociation from PICs. The kinetic constants of eIF1A dissociation from 43S AUG or UUG complexes from panel 3B are shown in Table 1. (C) Effect of the eIF5-Quad mutant on GTP-hydrolysis from 43S.AUG complexes. The eIF5-Quad mutant has no significant affect on GTP-hydrolysis (black squares), since the eIF5-Quad exhibits similar levels of hydrolysis when compared to wild-type eIF5 (red circles).
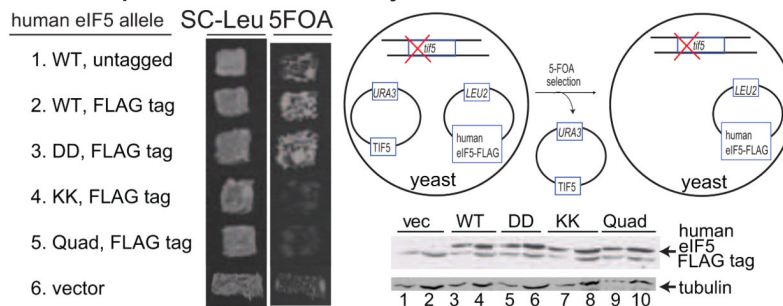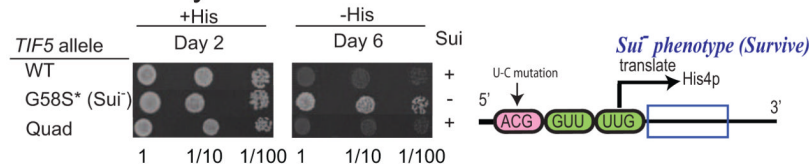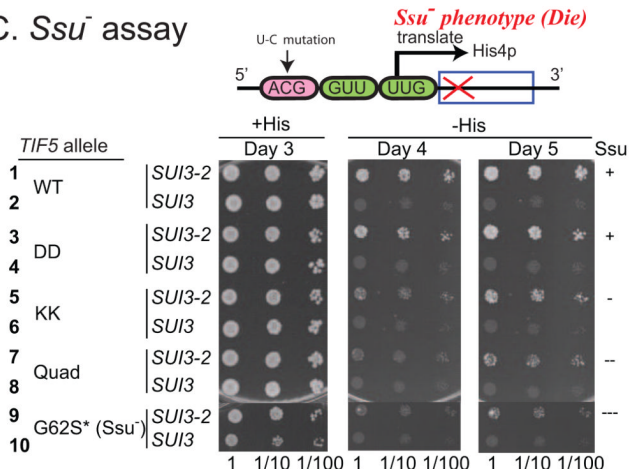
Figure 5. Genetic evidence that the KK and Quad substitutions disrupt a critical linkage with eIF2β and impairs the function of eIF5-CTD in promoting the closed complex
(A) Complementation of *tif5Δ* by single-copy human eIF5 plasmids in yeast (1. YCpL-heIF5, 2. YCpL-heIF5-FL, 3. YCpL-heIF5-DD-FL, 4. YCpL-heIF5-KK-FL, 5. YCpL-heIF5-DDKK-FL, 6. YCplac111). (Left) Patches of transformants of KAY24 (*tif5Δ* p[TIF5 URA3]) carrying the indicated plasmids were replica-plated onto SC-leu agar plates and SC agar plates containing 5-FOA and uracil, which was used to evict the residing TIF5 URA3 plasmid. Cells were allowed to grow on these plates for a few days. The schematic of FOA negative selection is shown on the right. 20 and 40 μg (odd and even numbered lanes, respectively) of cell extracts from the KAY24 transformants carrying YCplac111 (vec) or the indicated YCpL-heIF5-FL derivatives (Table S4) were subjected for immunoblotting with antibodies indicated to the right. Upper panel: Westerns using anti-Flag antibody to detect the relative expression levels of FLAG-tagged human eIF5 proteins (top bands; bottom bands are cross-reactivity, also showing equal loading). Lower panel: Western blotting results showing comparable expression levels of a housekeeping protein, tubulin. (B) Test of suppressor of initiation (Sui⁻) phenotypes. *TIF5* alleles correspond to eIF5 alleles in yeast. A lack of Sui⁻ phenotype is represented by (+). Cultures (A_{600}=0.15) of KAY976 (*his4-306*) derivatives (Table S5) with indicated *TIF5* alleles and their dilutions indicated on bottom are spotted onto SD+Trp+Ura medium with (+His) or without (−His)

and incubated for indicated number of days. (C) Test of suppressor of suppressor of initiation (Ssu⁻) phenotypes against *SUI3-2* (eIF2β-S264Y). A lack of Ssu⁻ phenotype is represented by (+). KAY976 (*his4-306*) derivatives (Table S5) with indicated *TIF5* alleles carrying YCpU-SUI3-2 (*SUI3-2*) or YCpU-SUI3 (*SUI3*) control plasmid (Watanabe et al., 2010) were grown and spotted onto SC-Ura (+His) or SC-Ura-His (–His) as in (B) and incubated for indicated number of days. The (*) following G58S or G62 represent the numbering for yeast residues located in the N-terminal domain of *TIF5*.
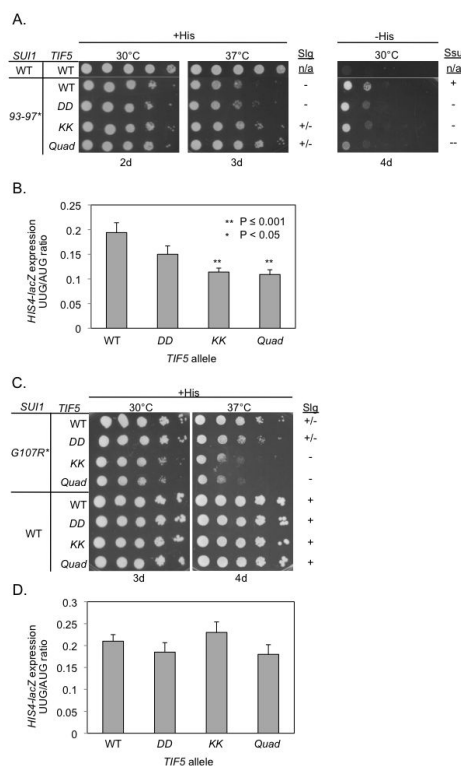
Figure 6. Genetic evidence that the KK and Quad substitutions impair eIF5-CTD function in releasing eIF1 from the closed complex

SUI1 and *TIF5* alleles correspond to yeast *eIF1* and *eIF5* alleles, respectively. (A-B) The *TIF5 KK* and *Quad* mutations suppress the Slg⁻ (slow-growth) and Sui⁻ phenotypes of *sui1-93-97*. A lack of Sui⁻ or Slg⁻ phenotype is represented by (+). Derivatives of *sui1Δ his4-301 P_GAL-TIF5* strain PMY01 harboring *sui1-93-97* and the indicated plasmid-borne *TIF5* alleles, plus control strain PMY106 containing WT *SUI1* and WT *TIF5*, were spotted in 10-fold serial dilutions on synthetic dextrose complete (SC) medium supplemented with 0.3 mM histidine (+His) or lacking His (–His) and incubated for the indicated number of days. (B) Strains from (A) also harboring *HIS4-lacZ* reporter plasmids with an AUG (p367) or UUG (p391) start codon were cultured in synthetic dextrose minimal medium (SD) supplemented with His at 30°C to A_{600} of ~1.0, and β-galactosidase activities (nmol of o-nitrophenyl β-D-galactopyranoside cleaved per min per mg) were measured in whole cell extracts (WCEs). The ratio of expression of the UUG versus AUG reporter was calculated for replicate experiments, and the mean and S.E.M. (error bar) was plotted. The UUG/AUG ratios were determined to be significantly smaller in the *tif5-KK* and -*Quad* mutants versus WT *TIF5* strain by the Student's *t* test. (C-D). The *KK* and *Quad* mutations exacerbate the Slg⁻ phenotype and do not suppress the elevated UUG:AUG ratio, conferred by *sui1-G107R*. Transformants of the indicated genotype were examined for growth on SC +His medium in panel C, just as in (A), and for the UUG:AUG initiation ratio for *HIS4-lacZ* in panel D, just as in (B). The UUG/AUG ratios were not significantly different among the WT and mutant *TIF5* strains. The (*) following *SUI1* mutants (*93-97* and *G107R*) represent the numbering for residues located in yeast eIF1. The corresponding human eIF1 residues are the following (*V98-G101* and *G112*).
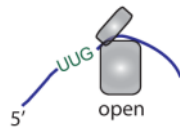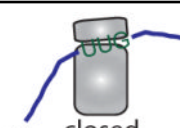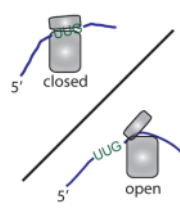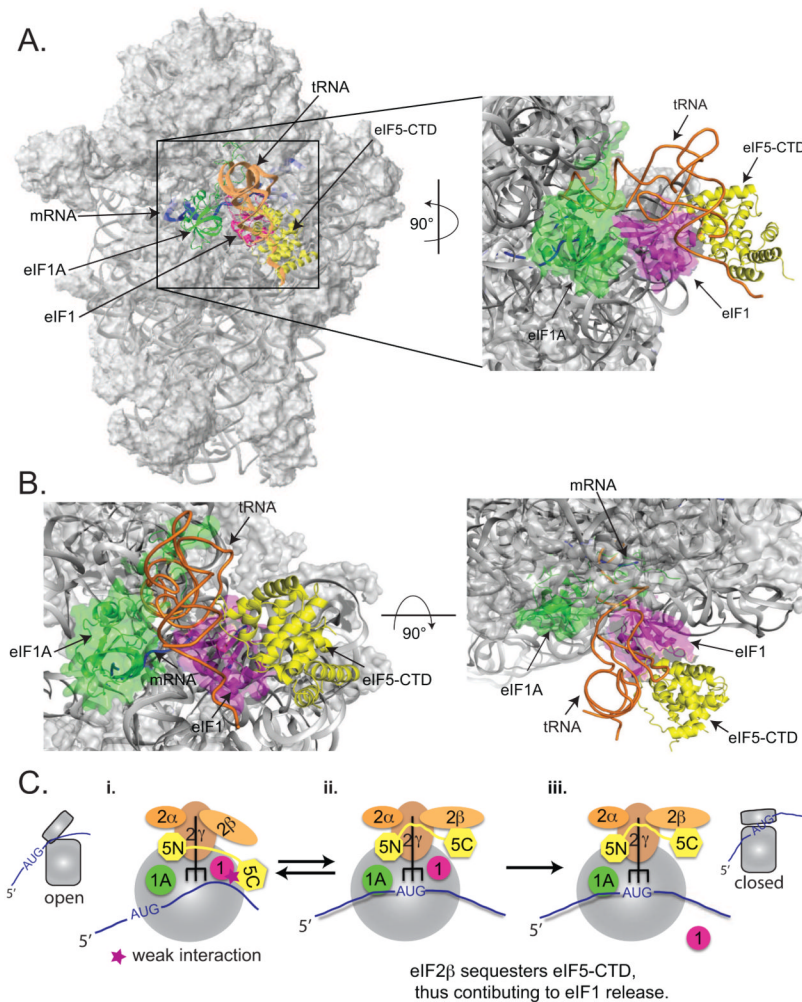
Figure 7. Modeling the eIF1:eIF5-CTD complex in the context of the eIF1:40S structure and schematic showing the role of eIF5-CTD in promoting start codon recognition

(A) The eIF1:eIF5-CTD complex derived from the HADDOCK software was superimposed on the position of human eIF1 on the small ribosomal subunit (Lomakin et al., 2003; Rabl et al., 2011), shown as a magenta ribbon. The modeled position of the human eIF5-CTD domain (yellow) was obtained by aligning eIF1 from the eIF1:eIF5-CTD complex (Figure 1G) to ribosome-bound eIF1. eIF1A (green), mRNA (blue) and P-site tRNA (orange) are also shown for reference. The P-site tRNA is shown in a P/P orientation. Note that the actual orientation of the ^{Met}tRNA$_i$ on the 40S subunit can not be exactly in a P/P orientation, since it would clash with eIF1 (Rabl et al., 2011) and is likely to change over the course of translation initiation. In the right panel, the modeled eIF1A:eIF1/eIF5-CTD:40S ribosomal complex was rotated 90° along the Y-axis and magnified. (B) In the left panel, the eIF1A:eIF1/eIF5-CTD:40S ribosomal complex is in the same orientation as the left panel of Figure 7A but magnified. In the right panel, the modeled eIF1A:eIF1/eIF5-CTD:40S ribosomal complex was rotated 90° along the X-axis from the left panel. (C) Schematic diagram of eIF5-CTD gating the release of eIF1 after start codon selection, followed by subsequent stabilization of the PIC by eIF5. (C-i.) The open 43S conformation allows for mRNA recruitment and relatively unstable eIF2-TC binding. During the assembly stage of the PIC, eIF5-CTD (HEAT) interacts with eIF1. (C-ii.) The 43S PIC scans the mRNA in an open conformation until start codon recognition. During this scanning stage, the eIF5-NTD

induces eIF2γ to cleave GTP. Start codon recognition sets the stage for large conformational rearrangements on the subunit interface ensuring the closed state of the PIC. eIF2β exhibits a stronger affinity for the overlapping binding surface of the eIF5-CTD than eIF1, hence the disruption of the eIF1:eIF5-CTD interaction by eIF2β allows for an indirect mechanism to dislodge eIF1 from the 43S PIC. Upon release of eIF1, the free phosphate is subsequently released. (C-iii.) eIF5-CTD stabilizes the closed ribosomal conformation of PICs upon start codon selection.

Table 1

Kinetic constants of eIF1A dissociation from 43S AUG/UUG complexes

eIF5 allele	AUG	UUG
WT	$k_1 = 9.0 \pm 3.0$; $a_1 = 0.14 \pm 0.06$ $k_2 = 0.35 \pm 0.05$; $a_2 = 0.86 \pm 0.2$ $K_{amp} = 6.1 \pm 1.5$ (a_2/a_1)	$k_1 = 7.0 \pm 3.0$; $a_1 = 0.33 \pm 0.1$ $k_2 = 2.0 \pm 0.5$; $a_2 = 0.67 \pm 0.2$ $K_{amp} = 2.5 \pm 0.5$
Quad	$k_1 = 30 \pm 7.0$; $a_1 = 0.49 \pm 0.05$ $k_2 = 2.5 \pm 0.5$; $a_2 = 0.51 \pm 0.1$ $K_{amp} = 1.5 \pm 0.5$	$k_1 = 60 \pm 10$; $a_1 = 0.44 \pm 0.1$ $k_2 = 7.2 \pm 1.0$; $a_2 = 0.56 \pm 0.05$ $K_{amp} = 1.2 \pm 0.2$
k_1 = fast phase rate constant a_1 = fast phase amplitude	Fast phase signifies open state	
k_2 = slow phase rate constant a_2 = slow phase amplitude	Slow phase signifies closed state.	
$K_{amp} = a_2/a_1$ = closed/open	K_{amp} is the ratio of closed to open state.	

All rates are 10^{-3} s^{-1}.